Fachtagung "Experimentelle Strömungsmechanik"
4. – 6. September 2018, Rostock

Bestimmung der Fluid-Partikel Relativgeschwindigkeiten in mikrofluidischen Suspensionsströmungen mittels Mikro-PIV

Determination of fluid-particle slip velocities of microfluidic suspension flows by means of micro-PIV

Sebastian Blahout, Jeanette Hussong
AG Lasermesstechnik der Mehrphasenströmungen,
Lehrstuhl für Hydraulische Strömungsmaschinen,
Ruhr-Universität Bochum

µPIV, Suspensionsströmung, Brechungsindexanpassung
µPIV, Suspension flows, refractive index matching

Abstract
We report on fluid-particle slip velocity measurements in a microfluidic suspension flow. For this, PMMA suspension particles and standard PS µPIV tracers are suspended in the carrier fluid. As the suspension particles are fluorescently labelled and refractive index matched to the carrier fluid, they assume ring-shaped particle images while remaining transparent in the particle centre. Measurements are performed in a microchannel for different Reynolds numbers with particle volume fractions up to 10 Vol.-%.
Utilising suspension particles with ring-shaped particle images, we present measurements on fluid-particle slip velocities as well as actually present particle volume fractions as a function of the channel height.

Introduction
Fluid-particle slip velocities are a key mechanism determining the transport of both liquid and solid phase. In laminar micro flows, fluid-particle slip velocities are commonly known to originate from gravity effects or stick-slip dynamics of particles along walls. However, in the presence of strong velocity gradients, particle Reynolds numbers may become sufficiently high to observe inertial particle dynamics that leads to a relative drift motion between particles and surrounding liquid. One of the most prominent examples is the lateral migration effect of singular particles in a tube flow, already shown in the 1960s by Segré and Silberberg [Segré and Silberberg, 1962]. Nowadays, single particle dynamics in dilute laminar suspension flows is well describable. The prediction of semi-dilute and dense suspension flows in microfluidic geometries is still ongoing research and almost exclusively subject to numerical studies up to date [Dhont et al., 2008; Maranzano and Wagner, 2002; Costa et al., 2017]. Recently, various inertial migration driven particle allocation patterns could be observed numerically in neutrally buoyant microfluidic suspension flows of 1-10 Vol.-% seeding density [Kazerooni et al., 2017]. While these simulations utilise a lubrication approach to account for particle-particle and particle-wall interactions [Costa et al., 2015], more complex surface properties such as roughness, strong surface elasticity due to material swelling or surface charges are not considered.
However, for future technical applications e.g. in process and chemical engineering, it is crucial to gain a more detailed understanding of such systems. Recent research efforts aim to utilize the migration of inertial micro particles for highly selective fractionation principles of micro particles smaller than 10µm [Fan et al., 2014; Huang, 2004; Zhang et al., 2015]. For applicable technological developments however, alternative or complementing routes to cost-expensive

Karlsruhe, Germany, ISBN 978-3-9816764-5-7

parallelisation of systems such as increased throughput rates or higher seeding densities of particles need to be exploited.
The aim of the present study is to investigate the influence of particle volume fraction on the fluid-particle slip velocity for rectangular duct flows. For this, an experimental procedure has been established to realise an optically accessible suspension flow while being able to perform µPIV measurements on both suspension particles and neutrally buoyant fluid tracers. In preceding studies, we could show that refractive index matching and fluorescent labelling of suspension particles results in ring-shaped particle images that allow to maintain a good optical accessibility to the flow but also appear to be suitable for µPIV measurements. In a comparison of synthetic image data ring-shaped particle images outperformed particles of the same image diameter and classical Gaussian intensity distribution in terms of detectability and displacement estimation error [Blahout and Hussong, 2017]. With the current work the theoretical study is extended to experimental investigations of a refractive index matched suspension flow of fluorescently labelled particles in a rectangular micro channel. For this, relative velocities of suspension particles and the carrier fluid are measured simultaneously for different particle volume fractions.

Set-up and Measurement Procedure
For all measurements a standard µPIV set-up is used, consisting of an epifluorescent upright microscope (Nikon Eclipse LV100), a double pulsed Nd:YAG Laser (Quantel Evergreen 70) with a wavelength of λ = 532nm and a double-frame CCD camera (LaVision Imager SX 5M).
The channel geometry, that is used during all measurements, has a height of h = 270µm, a width of w = 1mm and a length of l = 58mm.
The carrier fluid that is used throughout all investigations, is a ternary mixture of water, Glycerine and Ammoniumthiocyanate [Bailey and Yoda, 2003]. This results in a fluid with a density and refractive index that is matched to Polymethylmethacrylat (PMMA) suspension particles.
For the present study a monodisperse suspension of PMMA particles with a particle diameter of $D_{P,SUS}$ = 60µm is used. These originally transparent particles become visible through a labelling procedure, using a molecular Rhodamine B dye. For a magnification of M = 7 and a pixel size of 3.45µm, this results in a ring-shaped particle image of $D_{PID,SUS} \approx$ 140px, see Figure 1.

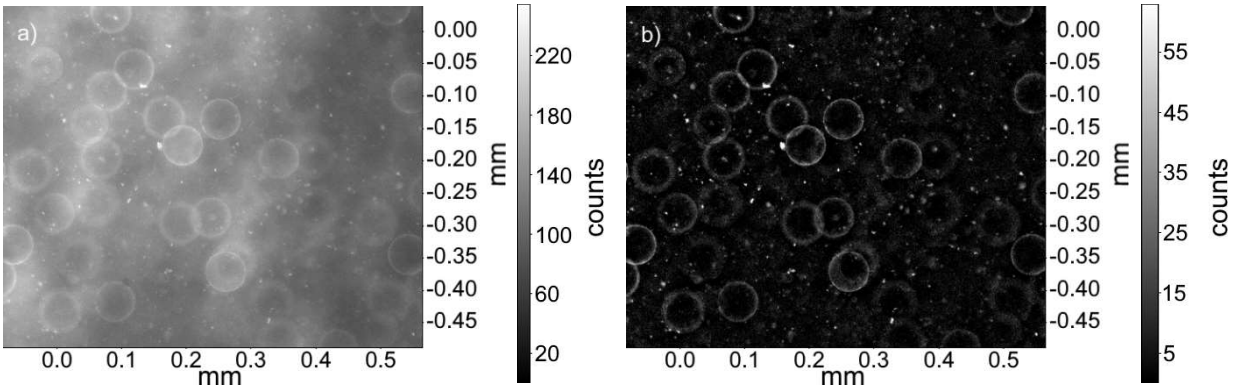

Figure 1: Recorded image of a ternary mixture of water, glycerine and Ammoniumthiocyanate with suspension particles of $D_{P,SUS}$ = 60µm and tracer particles of $D_{P,PIV}$ = 1.19µm: **a)** Raw recorded image; **b)** Pre-processed image.

Additionally, PEG coated µPIV tracer particles with a diameter of $D_{P,PIV}$ = 1.19µm (microparticles GmbH) are added to the fluid. In combination with the used microscope objective (Nikon CFI60 Infinity Corrected) of magnification M = 10, this results in a depth of correlation of $\delta_{DOC,10}$ = 27.43µm for Gaussian particles images [Olsen and Adrian, 2000].
For investigations of the relative velocity between the suspension particles and the channel flow, measurements have been performed at suspension particle volume fractions of Φ_N = 2.5% and 10% and a bulk Reynolds number of Re = 1. Here, the bulk Reynolds number is calculated as:

Karlsruhe, Germany, ISBN 978-3-9816764-5-7

$$Re = \frac{\rho \cdot U \cdot D_h}{\mu}$$

with D_h being the hydraulic diameter of the channel and U the mean flow velocity in main flow direction. The corresponding particle Reynolds number is defined as [Fan et al., 2014]:

$$Re_{P,SUS} = \frac{\rho \cdot U_m \cdot D_{p,SUS}^2}{\mu \cdot D_h}.$$

Here ρ denotes the fluid density and U_m the maximum fluid velocity in main flow direction, which is defined as $U_m = \frac{3Q}{2A}$, with the volume flow rate Q and the channel cross section A. This results in a particle Reynolds number of $Re_P = 0.017$ for a bulk Reynolds number of Re = 1.
For Re = 1 two different particle volume fractions $\Phi_{N,1} = 2.5\%$ and $\Phi_{N,1} = 10\%$ are realised and flow profiles in the middle of the channel side walls at an upstream position of x = 28mm from the inlet are measured. Starting at the bottom of the channel, z = 0µm, the microscope head is traversed in Δz = 30µm steps through the channel, resulting in nine measurement planes over the channel height.

Data Evaluation
On every recording set, consisting of N = 250 images, a subtract minimum over time filter is applied to the data set to reduce background noise. Afterwards, a non-linear sliding average filter with a filter length of $L_1 = 1.5$ pixel and a Gaussian weighting function is used to reduce salt-and-pepper noise. In a last step, the remaining image noise is reduced with the help of a spatial subtract sliding minimum filter with a filter length of $L_2 = 20$ pixel.
The pre-processed image data is separated by a Matlab (MathWorks) algorithm, resulting in two image sets containing only µPIV tracers on the one hand and suspension particles on the other hand (see Figure 2a and b). Images of µPIV tracers contain $3 \cdot 10^{-4}$ particles per pixel.
Separated image data sets are evaluated using a commercial ensemble average cross-correlation algorithm (LaVision DaVis 8.4.0). For this, multi-pass options with a decreasing interrogation window size are applied. During the first evaluation loop, an interrogation window size of 256 x 256 pixel is used, afterwards two additional loops with an interrogation window size of 128 x 128 pixel are performed with 50% interrogation window overlap. Based on the resulting correlation data, vectors with a detectability below 2 are deleted. Furthermore, a universal outlier detection is performed and empty vector spaces are filled up by interpolation replacing approximately 1-2% of the vector results.

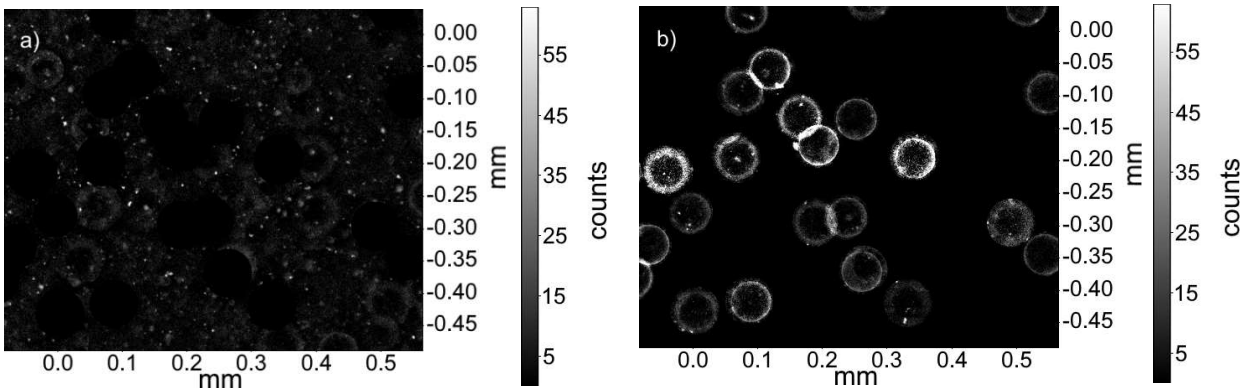

Figure 2: a) Pre-processed recording image; **b)** Separated µPIV tracer image ($D_{P,PIV}$ = 1.19µm); **c)** Separated suspension particles image ($D_{P,SUS}$ = 60µm).

The suspension particle volume fraction is calculated by dividing the volume of all suspension particles in the particular image by the measurement volume, assuming a measurement volume thickness of Δz = 60µm, i.e. one particle diameter. This is about one order of magnitude larger than the depth of focus of the used microscope objective.

Results and Discussion

The results of the measurements described above are shown in this section. Specifically, we present results on the spatial fluid and suspension particle velocities, as well as suspension particle volume fraction as a function of the channel height.

Spatial distribution of fluid-particle slip velocities and suspension particle volume fraction

The resulting flow profiles for suspension particle volume fractions of Φ_N = 2.5% and Φ_N = 10%, as well as the measured particle volume fraction at Re = 1 are shown as a function of the channel height in Figure 3 and Figure 4.

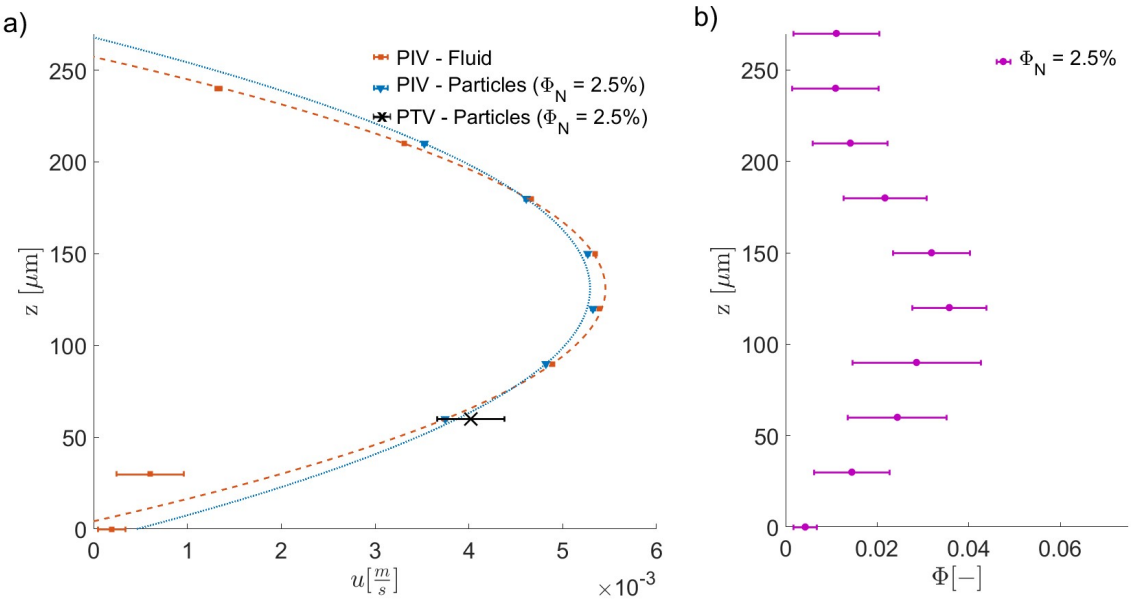

Figure 3: a) Velocity of carrier fluid (dashed curve) and suspension particles (solid curve) as a function of the channel height for Φ_N = 2.5%, including a PTV velocity result at z = 60µm; **b)** Measured particle volume fraction as a function of the channel height.

Based on the measurements shown in Figure 3a) suspension particles (solid curve) seem to be slower in the middle of the channel between 75 < z < 175µm than the carrier fluid (dashed curve). Towards the bottom and the top wall suspension particles seem to become faster compared to the carrier fluid. Furthermore, an increase of suspension particle volume fraction towards the middle of the channel is measured as shown in Figure 3b).

Figure 4a) shows velocities of suspension particles (solid curve) and carrier fluid (dashed curve) for a rectangular channel flow at Re = 1 with a suspension particle volume fraction of Φ_N = 10%. Here, suspension particles appear to have the same velocity as the carrier fluid in the middle region of the channel (95 < z < 155µm) while they appear to be faster than the fluid towards the channel bottom and top walls. Similar trends of fluid-particle slip velocities have been observed in fully resolved simulations of laminar suspension flow in ducts with Φ = 5 – 20% and a similar particle to channel height of $h/D_{P,SUS}$ = 18 [Kazerooni et al., 2017].

We hypothesise that the reason for particles to be faster than the flow near walls while being slower in the bulk of the flow might be a momentum transfer between particles from the bulk towards wall close particles.

For high particle volume fractions, this is known to result in a plug flow profile [Karnis et al., 1966]. Another possible explanation for slip velocities especially in the bulk may be finite particle size effects due to large particle to channel height ratios and the presence of curvature in

Karlsruhe, Germany, ISBN 978-3-9816764-5-7

the flow profile, inducing Faxén forces [Guazzelli et al., 2012]. To test these hypotheses, further investigations at larger particle volume fractions and higher particle to channel height ratios are planned.

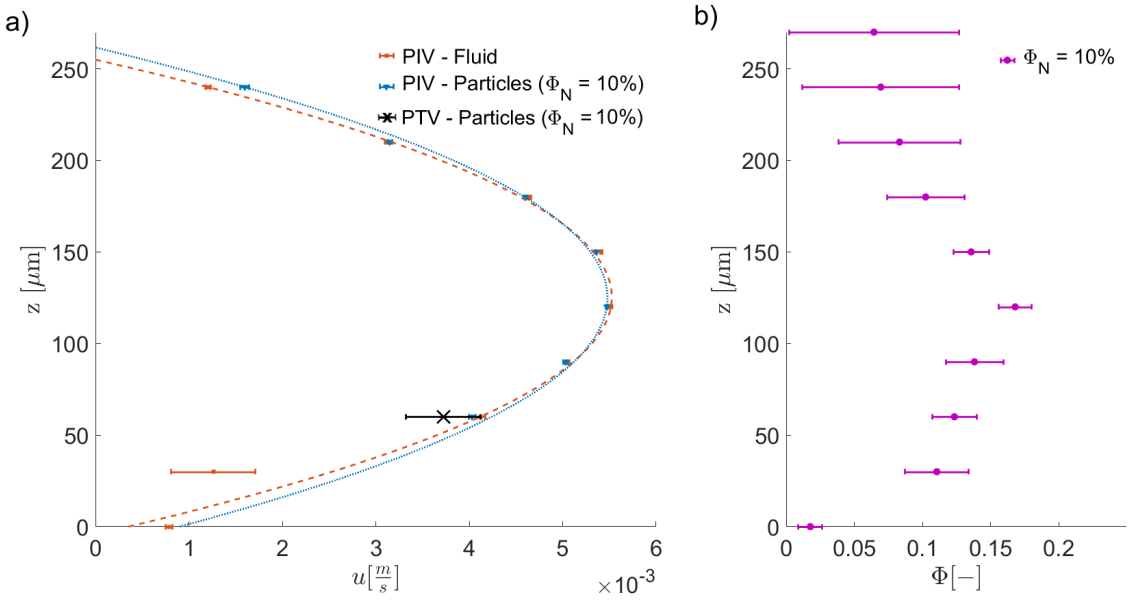

Figure 4: a) Velocity of carrier fluid (dashed curve) and suspension particles (solid curve) as a function of the channel height for Φ_N = 10%, including PTV velocity results at z = 60µm; **b)** Measured particle volume fraction as a function of the channel height.

The distribution of suspension particles over the channel height for Φ_N = 10% is qualitatively similar to that of Φ_N = 2.5% (Figure 3a). A maximum particle volume fraction of Φ = 16.8 ± 1.2% is measured at a channel height of z = 120µm for the Φ_N = 10% case.
An inhomogeneity of particle volume fractions over the channel height can be explained by slight density differences between carrier fluid and suspension particles, which leads to a sedimentation of the latter. While the sedimentation velocity is slower than the bulk velocity in main flow direction, suspension particles located in the middle plane of the channel will reach the measurement volume nearly at the same height as they are convected faster downstream and therefore have travelled only a small distance in lateral direction due to gravity forces. Particles located at the top and bottom wall move much slower downstream due to slow fluid velocities. These particles have much more time to sediment before reaching the measurement volume. Particles located near the bottom wall may even stick at the bottom. This leads to a depletion effect of particles near top and bottom wall while higher volume fractions are reached in the bulk of the flow.
Furthermore, first investigations on the dependence of the slip velocity as a function of the bulk Reynolds number have been performed at z = 150µm up to Re = 75 (Re_P = 1.264). These results show an increase of the fluid-particle slip velocity with increasing bulk Reynolds number. As both, a dependence of the slip velocity, as well as of the particle volume fraction at this channel height was detected, further investigations are required at higher Reynolds numbers, as well as different particle volume fractions and channel height positions to gain a more complete picture of the Reynolds number effect on the suspension dynamics.

Comparison of µPIV and PTV results

µPIV measurements have been performed up to a spacing of one suspension particle diameter to the walls (z = 60 µm wall spacing). As µPIV measurements are usually biased near walls, due to high velocity gradients and an inhomogeneous particle concentration over the correlation depth, a PTV evaluation has been additionally applied to the pre-processed data set of suspension particle images at $z/D_{P,SUS}$ = 1. In Figure 3a) and Figure 4a) median values of the PTV (marked with an **x**) and µPIV evaluation are displayed, respectively.

Karlsruhe, Germany, ISBN 978-3-9816764-5-7

Both evaluation procedures display the same median suspension velocity at $z/D_{P,SUS} = 1$. Thus, no bias error can be observed in the present study for µPIV measurements performed with suspension particles. We assume that this is due to the fact that the correlation depth of the ring-shaped particle images used – also at measurement planes close to the wall – never reaches outside of the flow domain in the present study. This is possible as refractive index matched suspension particles with ring-shaped particle images are used here. Due to their particle image characteristics they defocus faster than corresponding Gaussian particle images. This reduces the correlation depth significantly such that the correlation depth equals or even shrinks below twice the particle diameter. Therefore, a bias error due to inhomogeneous particle distribution over the measurement volume depth, i.e. the correlation depth close to walls can be avoided. Of course, this is true only if a physically meaningful minimum spacing of at last one suspension particle radius is chosen between wall and focal plane.
Based on recent results we assume that particles of ring-shaped image rather scale with the ring width itself, than with their actual particle image diameter (which is the case for Gaussian µPIV particle images, see [Olsen and Adrian, 2000]). Future studies aim to work out a proper length scale that provides a scaling relation between ring-shaped particle images and apparent correlation depth.

Conclusion and Outlook

To gain optical access into neutrally buoyant microfluidic suspension flow, refractive index and density matching has been applied to suspended 60µm PMMA suspension particles. Fluid-particle slip velocities could be successfully measured up to a nominal suspension particle volume fraction of $\Phi_N = 10\%$. This was possible as suspension particles were visible only at their circumference while remaining transparent in their centre. In this way a good optical access to the flow is ensured such that also small, neutrally buoyant fluid tracers of 1.19µm diameter remain visible over the whole micro channel height of 270µm.
For a defined bulk Reynolds number of $Re = 1$, slip velocity distributions were measured at nominal particle volume fractions of $\Phi_N = 2.5\%$ and $\Phi_N = 10\%$. In agreement with recent numerical studies [Kazerooni et al. 2017] we found that suspension particles appeared to be slightly slower in the channel bulk, while they are faster at wall close regions for a spacing between wall and focal plane of less than 1.5 particle diameters.
An increase of slip velocities was observed in the middle of the channel for rising bulk Reynolds numbers up to $Re = 75$. Further measurements are required over the whole channel height at higher bulk Reynolds numbers to confirm or debunk this trend.
As refractive index matched suspension particles appear as ring-shaped particle images, they show a stronger defocusing effect that reduces the measurement volume thickness to a point that bias errors due to a finite depth of correlation can be avoided. Recent results suggest that for ring-shaped particle images the correlation depth is of the order of the particle diameter itself. Further studies will also aim at determining an apparent depth of correlation for ring-shaped particle images in more detail.

Literature

Segré, G. and Silberberg, A., 1962: 'Behaviour of Macroscopic Rigid Spheres in Poiseuille Flow Part 1. Determination of Local Concentration by Statistical Analysis of Particle Passages through Crossed Light Beams', Journal of Fluid Mechanics 14, no. 01: 115.
Segré, G. and Silberberg, A., 1962: 'Behaviour of Macroscopic Rigid Spheres in Poiseuille Flow Part 2. Experimental Results and Interpretation', Journal of Fluid Mechanics 14, no. 01: 136.
Kazerooni, H. Tabaei, Fornari, W., Hussong, J., Brandt, L., 2017: 'Inertial Migration in Dilute and Semidilute Suspensions of Rigid Particles in Laminar Square Duct Flow', Physical Review Fluids 2, no. 8.
Costa, P., Boersma, B. J., Westerweel, J., Breugem, W.-P., 2015: 'Collision Model for Fully Resolved Simulations of Flows Laden with Finite-Size Particles', Physical Review E 92, no. 5.
Dhont, J.K.G. and Briels, W.J., 2008: 'Gradient and Vorticity Banding', Rheologica Acta 47, no. 3: 257–81.

Karlsruhe, Germany, ISBN 978-3-9816764-5-7

Maranzano, B.J. and Wagner, N.J., 2002: 'Flow-Small Angle Neutron Scattering Measurements of Colloidal Dispersion Microstructure Evolution through the Shear Thickening Transition', The Journal of Chemical Physics 117, no. 22: 10291–302.
Costa, P. et al., 2017: 'Finite Size Effects in Dense Turbulent Wall-Bounded Transport of Neutrally-Buoyant Spheres', ArXiv Preprint ArXiv:1703.06036.
Fan, L.-L., He, X.-K., Han, Y., Du, L. Zhao, L., Zhe, J. 2014: 'Continuous Size-Based Separation of Microparticles in a Microchannel with Symmetric Sharp Corner Structures', Biomicrofluidics 8, no. 2.
Huang, L.R. 2004: 'Continuous Particle Separation Through Deterministic Lateral Displacement', Science 304, no. 5673: 987–90.
Zhang, J., Yan, S., Sluyter, R., Li, W., Alici, G., Nguyen, N.-T., 2015: 'Inertial Particle Separation by Differential Equilibrium Positions in a Symmetrical Serpentine Micro-Channel', Scientific Reports 4, no. 1.
Blahout, S. and Hussong, J., 2017: 'Reduced Estimation Error of Cross-Correlation Based Displacements of Refractive Index Matched and Surface Labelled Suspension Particles', Fachtagung Experimentelle Strömungsmechanik 2017, ISBN 978-3-9816764-3-3: 31.
Bailey, B.C. and Yoda, M., 2003: 'An Aqueous Low-Viscosity Density- and Refractive Index-Matched Suspension System', Experiments in Fluids 35, no. 1: 1–3.
Olsen, M. G. and Adrian, R. J., 2000: 'Out-of-Focus Effects on Particle Image Visibility and Correlation in Microscopic Particle Image Velocimetry', Experiments in Fluids 29, no. 1, S166–S174.
Guazzelli, E., Morris, J. F., Pic, S., 2012: *A Physical Introduction to Suspension Dynamics*, Cambridge Texts in Applied Mathematics (Cambridge ; New York: Cambridge University Press).
Karnis, A., Goldsmith, H.L., Mason, S.G., 1966: 'The Kinetics of Flowing Dispersions', Journal of Colloid and Interface Science 22, no. 6: 531–53.

Karlsruhe, Germany, ISBN 978-3-9816764-5-7